C. R. Mecanique 344 (2016) 225–235

Contents lists available at ScienceDirect

Comptes Rendus Mecanique

www.sciencedirect.com

Computational simulation of manufacturing processes

# In-plane/out-of-plane separated representations of updated Lagrangian descriptions of viscoplastic flow models in plate domains

Diego Canales [a,b,*], Adrien Leygue [a], Francisco Chinesta [a], Icíar Alfaro [b], David González [b], Elías Cueto [b], Éric Feulvarch [c], Jean-Michel Bergheau [c]

[a] GeM, École centrale de Nantes, 1, rue de la Noë, 44321 Nantes, France
[b] I3A, Universidad de Zaragoza, Maria de Luna 3, 50018 Zaragoza, Spain
[c] University of Lyon, ENISE, LTDS, UMR 5513 CNRS, 58, rue Jean-Parot, 42023 Saint-Étienne cedex 2, France

ARTICLE INFO

*Article history:*
Received 23 February 2015
Accepted 3 April 2015
Available online 17 February 2016

*Keywords:*
Separated representation
PGD
Updated Lagrangian
SCNI

ABSTRACT

A new efficient updated Lagrangian strategy for numerical simulations of material forming processes is presented. The basic ingredient is the tensorial decomposition of the velocity field into a finite sum of in-plane and an out-of-plane components, giving rise to an equivalent computational complexity of some two-dimensional problems and some one-dimensional ones (therefore, much less than the true three-dimensional complexity of the original problem). This is efficiently achieved by using Proper Generalized Decomposition (PGD) techniques, which are here employed in an updated Lagrangian framework for the very first time. This updated Lagrangian nature of the method needs the use of a robust numerical integration technique (in this case, the Stabilized Conforming Nodal Integration has been chosen) for addressing the highly distorted projected meshes. The resulting strategy is of general purpose, although it is especially well suited for addressing models defined in plate or shell (in general, parallelepipedic) domains. The basics of the just-developed method are shown, together with some numerical examples to show the potential of the technique.



## 1. Introduction

The numerical simulation of material-forming processes is a fundamental tool in the industry. It allows reducing the design cycle time and optimizing the process with no need for costly and time-consuming test campaigns [1]. However, it continues to be a very challenging task, despite the high-performance computation hardware and software available nowadays. In addition, the simulation of processes defined in plate-like domains, possibly of very small thickness, such as co-extrusion or friction stir welding (FSW), involves some additional difficulties:

- the multiphysic nature of the problem. This leads to thermomechanical coupled problems with non-trivial boundary conditions,
- the presence of large transformations and, therefore, very distorted meshes when considering a Lagrangian framework,

* Corresponding author.
*E-mail addresses:* diego.canales-aguilera@ec-nantes.fr (D. Canales), francisco.chinesta@ec-nantes.fr (F. Chinesta).

http://dx.doi.org/10.1016/j.crme.2015.12.006
1631-0721/

- the simulation of voids and flaws,
- the presence of evolving free surfaces and fixed or moving interfaces,
- the need for the knowledge of the thermomechanical history of each material particle for evaluating properties depending on such thermomechanical history.

Moreover, modern industries demand a new paradigm in numerical simulation in order to improve their competitiveness. This new paradigm leads to the creation of virtual test platforms or to the online control of processes in real-time.

In general, three numerical simulation frameworks can be found in the literature. Choosing a particular one depends on the application and has a great influence on the former discussion about difficulties and new simulation challenges. Briefly, we can summarize the following frameworks.

- *Eulerian*. The discretization mesh is fixed. This means that the mesh does not evolve in time. In practice, with this approach, no mesh distortion occurs. This is, in principle, the easiest approach for simulating fluid-like materials with no free boundaries.
  Unfortunately, the material derivative in a fixed reference frame will contain a convective term. This convective term, when it dominates the problem, leads to numerical instabilities, and the problem should be stabilized [2]. Additionally, the path and the thermomechanical history of the material particles should be reconstructed *a posteriori*, which involves numerical inaccuracies. Moreover, this reconstruction should be frequent since the physics of the problem depends on the material distribution [3]. Finally, the treatment of free surfaces and evolving boundary conditions is a tricky issue within the Eulerian framework.
- *Lagrangian*. The discretization nodes are attached to material particles. The mesh evolves in time when following the material motion, thus their thermomechanical history is obtained directly. Free surfaces are easily tracked and boundary conditions imposed in a simple way [4–7].
  However, this approach leads to distorted meshes when large deformations occur, and therefore a frequent remeshing is needed. 3D-remeshing could be very expensive in practice, constituting for some applications the true bottleneck of the simulation. In addition, frequent projections of the fields between the old and new meshes are required, introducing numerical diffusion (unless some type of meshless formulation is employed, alleviating the remeshing needs, see [8]).
- *Arbitrary Lagrangian–Eulerian (ALE)*. This framework was developed in order to avoid the main issues of the former approaches while preserving their main advantages. The discretization nodes are attached neither to the space nor to the material points. The mesh moves in a prescribed way to avoid any excessive distortion, alleviating remeshing procedures.
  However, convective terms associated with the relative velocity between the mesh and the material remain in the formulation, implying again numerical difficulties. ALE-based methods can be very expensive in computational terms, and the field projection between meshes is not completely avoided. Moreover, they require a certain amount of "know-how": the mesh velocity depends on the specific application and its determination is not a trivial task. In any case, computational codes based on ALE approaches are widely considered for the numerical simulation of material-forming processes [9,10].

The choice of one or another approach will depend on the specific application. The interested reader can find a deeper analysis of these frameworks in [11]. For some specific forming procedures, such as Friction Stir Welding, for instance, different strategies may appear, which are better suited for different regions of the domain (Eulerian around the pin, Lagrangian faraway) [3] or simply updated Lagrangian [12] in the whole domain.

In many (if not all) material-forming simulations, because their inherent difficulties already mentioned, updated Lagrangian frameworks are very appealing. However, their computational cost remains sometimes too high, even for recent meshless strategies in the field [13]. Precisely, the main goal of this work is to explore new strategies to enhance updated Lagrangian simulations and to reduce substantially its computational cost. To that end, in Section 2 the main ingredients of the proposed technique are introduced, namely the space decomposition within the Proper Generalized Decomposition [14–17] and the use of efficient stabilized nodal conforming integration [18] to allow for minimal loss of accuracy despite mesh distortion [13,19]. In Section 3, the proposed strategy is validated, while in Section 4 the possibility of employing the proposed technique in more complex situations is studied.

## 2. Proposed strategy

The proposed strategy can be seen as a natural extension of the in-plane/out-of-plane tensorial decomposition based on the Proper Generalized Decomposition (PGD) to an updated Lagrangian framework. The idea of decomposing three-dimensional fields (here, velocity) into a sequence of two-dimensional and one-dimensional fields (the so-called finite sum decomposition, see [17]), is at the heart of the Proper Generalized Decomposition, PGD, and was initially developed for analyzing plates by B. Bognet et al. [20]. It has also been used in Eulerian frameworks to simulate solids and non-Newtonian fluids [21] with impressive savings of computational cost compared with traditional 3D FE methods.

The main idea of the approach developed here is to take advantage of updated Lagrangian methods, very convenient for material-forming simulations, in which the thermomechanical history is of major interest, but obtaining a significant

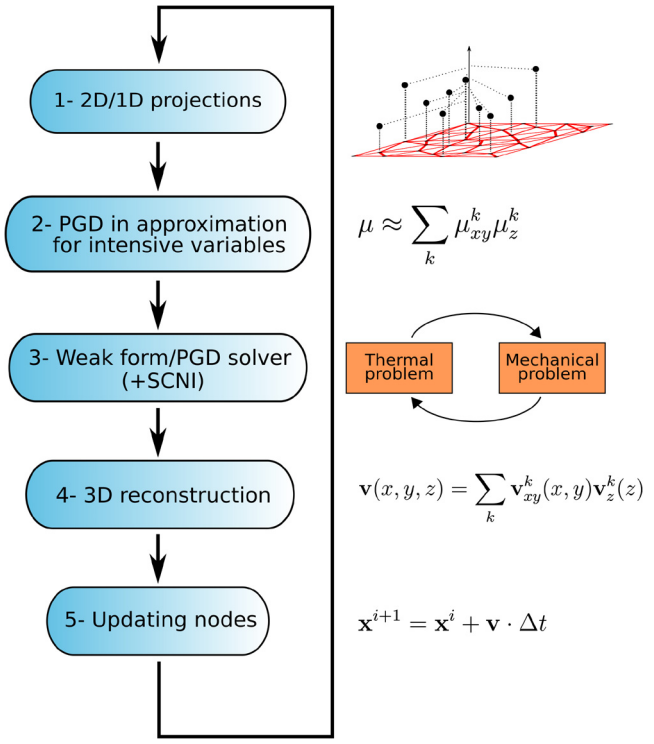


**Fig. 1.** General scheme of the proposed strategy.

reduction of its computational complexity using the in-plane/out-of-plane PGD-based decomposition. This will allow 3D solutions with a typical computational complexity characteristic of 2D simulations. The material particles' position and all the variables attached to them are projected onto a plane and onto the thickness axis (step 1). Using these nodal projections, two functional spaces are constructed, 2D and 1D, respectively. The intensive variables are projected on these spaces using a PGD approximation, equivalent to a singular value decomposition (SVD) (step 2). Then, the thermomechanical problem is solved as a series of 2D and 1D problems in these spaces thanks to the in-plane/out-of-plane PGD-based formulation (step 3). Once the solution is obtained, the primary variables can be reconstructed for the material particles in the 3D domain (step 4) and their positions updated (step 5). This reconstruction does not involve any interpolation or projection stage, thus avoiding numerical diffusion and other numerical difficulties. These steps are repeated until the end of the simulation. In Fig. 1, a general scheme of the strategy with its different steps is shown. Note that both the mechanical and the thermal parts of the problem can be solved using the spatial decomposition regardless of the coupling scheme used.

The main ingredients of the proposed strategy are presented in detail below. In Section 2.1, the space decomposition in the updated Lagrangian framework is described. A general flow model for material-forming processes is presented, considering linear and non-linear behavior laws. In Section 2.2, stabilized conforming nodal integration (SCNI) techniques are briefly reviewed, which allow performing an accurate integration of the operators, even in very distorted meshes [18,19].

### *2.1. The in-plane/out-of-plane decomposition in an updated Lagrangian framework*

Let us describe this updated Lagrangian strategy through a generic viscoplastic flow model [22] in a domain $\Omega$.

The balance of momentum and mass equations without inertia and the assumed incompressibility of the flow read:

$$\nabla \cdot \boldsymbol{\sigma} = \mathbf{0}, \quad \nabla \cdot \mathbf{v} = 0 \qquad \text{in} \quad \Omega \tag{1}$$

To calculate the temperature field, the viscoplastic flow model is coupled with the heat transfer equation:

$$\nabla \cdot (k \nabla T) + \dot{r} - (\rho c_p \dot{T}) = 0 \qquad \text{in} \quad \Omega \tag{2}$$

The rate of heat generation due to plastic deformation is obtained from

$$\dot{r} = \beta \sigma : \mathbf{d}$$

where $\beta$ is the fraction of mechanical energy transformed into heat and $\mathbf{d}$ the strain rate tensor.

Together with these equations, a constitutive law and the appropriate boundary conditions should be considered. The mechanical and thermal problem will be solved iteratively.

Considering a plate domain $\Omega = \Xi \times \mathcal{I}$ with $(x, y) \in \Xi$ and $z \in \mathcal{I}$, we assume the separated approximation of the velocity field

$$\boldsymbol{v}(x, y, z) = \begin{pmatrix} u(x, y, z) \\ v(x, y, z) \\ w(x, y, z) \end{pmatrix} \approx \sum_{i=1}^{N} \begin{pmatrix} u^i_{xy}(x, y) \cdot u^i_z(z) \\ v^i_{xy}(x, y) \cdot v^i_z(z) \\ w^i_{xy}(x, y) \cdot w^i_z(z) \end{pmatrix}$$

where $u_{xy}(x, y)$, $v_{xy}(x, y)$ and $w_{xy}(x, y)$ are function of the in-plane coordinates, whereas $u_z(z)$, $v^i_z(z)$ and $w_z(z)$ are functions involving the thickness coordinate. Similarly, the strain rate tensor can be expressed in separated form. For intensive variables, such as viscosity, the separated representation is performed by invoking again the PGD approximation, in that case equivalent to the SVD, as described in detail in chapter 3 of [14], which allows obtaining its in-plane/out-of-plane separated representation:

$$\mu(x, y, z) = \sum_{k=1}^{M} \mu^k_{xy}(x, y) \cdot \mu^k_z(z)$$

For obtaining this separated representation, we interpolate the viscosity at each position $((x, y)_i, z_k)$, with $i$ referring to the node associated with the in-plane mesh and $k$ the one associated with the thickness direction, which will be denoted by $\mu_{ik}$. Applying the SVD to the matrix $\mu_{ik}$, we obtain the in-plane and out-of-plane vectors, allowing us to write the above separated representation of the viscosity.

Two different constitutive laws have been considered. In the linear case, the constitutive equation reads:

$$\begin{cases} \nabla p = \mu \nabla \cdot (\nabla \mathbf{v}) \\ \nabla \cdot \mathbf{v} = 0 \end{cases}$$

where $p$ and $\mu$ are the pressure and the viscosity of the fluid, respectively.

To circumvent the problems related to the development of stable mixed formulations (i.e., approximations verifying the LBB condition) within the separated representation, a penalty formulation is considered, which modifies the mass balance by introducing a penalty coefficient $\lambda$ small enough

$$\nabla \cdot \mathbf{v} + \lambda p = 0$$

or, more explicitly,

$$p = -\frac{1}{\lambda}\left(\frac{\partial u}{\partial x} + \frac{\partial v}{\partial y} + \frac{\partial w}{\partial z}\right) = -\frac{\nabla \cdot \mathbf{v}}{\lambda}$$

By replacing it into the momentum balance (first equation in (1)), we obtain

$$\nabla (\nabla \cdot \mathbf{v}) + \xi \Delta \mathbf{v} = \mathbf{0}$$

with $\xi = \mu\lambda$. After some elementary algebra, it results

$$\begin{pmatrix} \frac{\partial^2 u}{\partial x^2} + \frac{\partial}{\partial x}\frac{\partial v}{\partial y} + \frac{\partial}{\partial x}\frac{\partial w}{\partial z} \\ \frac{\partial}{\partial y}\frac{\partial u}{\partial x} + \frac{\partial^2 v}{\partial y^2} + \frac{\partial}{\partial y}\frac{\partial w}{\partial z} \\ \frac{\partial}{\partial z}\frac{\partial u}{\partial x} + \frac{\partial}{\partial z}\frac{\partial v}{\partial y} + \frac{\partial^2 w}{\partial z^2} \end{pmatrix} + \xi \begin{pmatrix} \frac{\partial^2 u}{\partial x^2} + \frac{\partial^2 u}{\partial y^2} + \frac{\partial^2 u}{\partial z^2} \\ \frac{\partial^2 v}{\partial x^2} + \frac{\partial^2 v}{\partial y^2} + \frac{\partial^2 v}{\partial z^2} \\ \frac{\partial^2 w}{\partial x^2} + \frac{\partial^2 w}{\partial y^2} + \frac{\partial^2 w}{\partial z^2} \end{pmatrix} = 0$$

The *flow model* can readily be extended to power-law fluids:

$$\begin{cases} \nabla p = \nabla \cdot \mathbf{T} \\ \nabla \cdot \mathbf{v} = 0 \end{cases} \tag{3}$$

where the extra-stress tensor $\mathbf{T}$ writes:

$$\mathbf{T} = 2K\overline{d}^{n-1}\mathbf{d} \tag{4}$$

with $K$ and $n$ two rheological parameters and the equivalent strain rate $\overline{d}$ given by:

$$\overline{d} = \sqrt{2(\mathbf{d} : \mathbf{d})}$$

where ":" denotes the tensor product twice contracted.

In order to perform the in-plane/out-of-plane decomposition, the system of PDEs defined by Eqs. (1)–(2) should be written in its variational form. For instance, assuming linear behavior and a penalty formulation, the variational formulation writes:

$$a(\boldsymbol{w}, \boldsymbol{v}) + \xi b(\boldsymbol{w}, \boldsymbol{v}) = \mathbf{0} \tag{5}$$

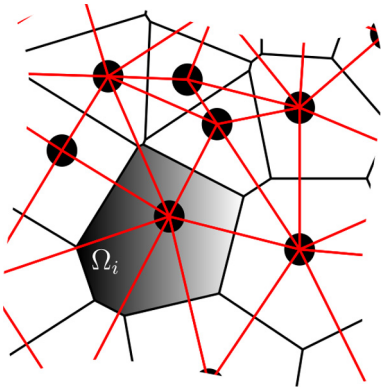


**Fig. 2.** Voronoi tessellation to perform the SCNI.

with

$$a(\boldsymbol{w},\boldsymbol{v})=\int_{\Omega}\nabla\cdot\boldsymbol{w}\,\nabla\cdot\boldsymbol{v}\,\mathrm{d}\Omega\quad\text{and}\quad b(\boldsymbol{w},\boldsymbol{v})=\int_{\Omega}\nabla\boldsymbol{w}:\nabla\boldsymbol{v}\,\mathrm{d}\Omega$$

where $a$ and $b$ are the bilinear forms related to the incompressibility and viscous terms; $\boldsymbol{v}$ and $\boldsymbol{w}$ are the trial and test functions, respectively.

Then, it is assumed that the first $n-1$ modes of the PGD solution have been previously obtained. To further enrich this solution with another functional product, the following problem needs to be solved:

$$\boldsymbol{v}(x,y,z)=\begin{pmatrix}u(x,y,z)\\v(x,y,z)\\w(x,y,z)\end{pmatrix}\approx\sum_{i=1}^{n-1}\begin{pmatrix}u^i_{xy}(x,y)\cdot u^i_z(z)\\v^i_{xy}(x,y)\cdot v^i_z(z)\\w^i_{xy}(x,y)\cdot w^i_z(z)\end{pmatrix}+\boldsymbol{R}(x,y)\circ\boldsymbol{S}(z)\tag{6}$$

where the second term on the right-hand side represents the enrichment and the symbol '$\circ$' denotes the so-called entry-wise Hadamard or Schur multiplication for vectors.

The test function is defined by:

$$\boldsymbol{w}=\boldsymbol{R}^*(x,y)\circ\boldsymbol{S}(z)+\boldsymbol{R}(x,y)\circ\boldsymbol{S}^*(z)\tag{7}$$

Introducing Eqs. (6) and (7) into Eq. (5), a non-linear problem results, due the presence of the products of the unknown PGD modes. This is the case even when the original problem is linear. To solve this non-linearity, an alternated-direction, fixed-point algorithm is used, which has proved to be simple and robust within the PGD framework [14,17].

### 2.2. FE-SCNI

In the proposed strategy, after nodal position updating, their orthogonal projections into a 2D domain defined by the in-plane coordinates and the 1D projection onto the domain thickness constitute the nodal position of the interpolant spaces used for the PGD solution. An additional problem is faced, since the 2D mesh will be, eventually, very distorted and the numerical integration of the discrete operators may be not accurate enough.

Chen et al. [18] introduced the SCNI technique to perform an accurate nodal integration in meshless methods. Indeed, it has been observed [19,13] that SCNI can be incorporated into traditional FE formulations to produce a very robust method to deal with highly distorted meshes with almost no loss of accuracy.

The SCNI is based on the assumed strain method, in which a modified gradient is introduced at the integration point (node):

$$\tilde{\nabla}\boldsymbol{v}(\boldsymbol{x}_i)=\frac{1}{A_i}\int_{\Omega_i}\nabla\boldsymbol{v}(\boldsymbol{x})\,\mathrm{d}\Omega$$

where $\boldsymbol{x}_i$ are the coordinates of node $n_i$ and $A_i$ the area defined by the cell $\Omega_i$. The set of cells defines a partition of the 2D domain. Typically, a Voronoi tessellation is used (see Fig. 2), although any type of non-overlapping tilling can be used.

The modified strain rate tensor is given by

$$\tilde{\boldsymbol{d}}(\boldsymbol{x}_i)=\frac{1}{A_i}\int_{\Omega_i}\boldsymbol{d}(\boldsymbol{x})\mathrm{d}\Omega=\frac{1}{A_i}\int_{\Omega_i}\begin{pmatrix}\frac{\partial u}{\partial x} & \frac{1}{2}\left(\frac{\partial u}{\partial y}+\frac{\partial v}{\partial x}\right) & \frac{1}{2}\left(\frac{\partial u}{\partial z}+\frac{\partial w}{\partial x}\right)\\ \frac{1}{2}\left(\frac{\partial u}{\partial y}+\frac{\partial v}{\partial x}\right) & \frac{\partial v}{\partial y} & \frac{1}{2}\left(\frac{\partial v}{\partial z}+\frac{\partial w}{\partial y}\right)\\ \frac{1}{2}\left(\frac{\partial u}{\partial z}+\frac{\partial w}{\partial x}\right) & \frac{1}{2}\left(\frac{\partial v}{\partial z}+\frac{\partial w}{\partial y}\right) & \frac{\partial w}{\partial z}\end{pmatrix}\mathrm{d}\Omega$$

Applying the divergence theorem, it results:

$$\tilde{\boldsymbol{d}}(\boldsymbol{x}_i) = \frac{1}{A_i}\int_{\Gamma_i} \begin{pmatrix} u(\boldsymbol{x})n_x & \frac{1}{2}(u(\boldsymbol{x})n_y + v(\boldsymbol{x})n_x) & \frac{1}{2}(u(\boldsymbol{x})n_z + w(\boldsymbol{x})n_x) \\ \frac{1}{2}(u(\boldsymbol{x})n_y + v(\boldsymbol{x})n_x) & v(\boldsymbol{x})n_y & \frac{1}{2}(v(\boldsymbol{x})n_z + w(\boldsymbol{x})n_y) \\ \frac{1}{2}(u(\boldsymbol{x})n_z + w(\boldsymbol{x})n_x) & \frac{1}{2}(v(\boldsymbol{x})n_z + w(\boldsymbol{x})n_y) & w(\boldsymbol{x})n_z \end{pmatrix} \mathrm{d}\Gamma$$

Thus, in order to compute the strain rate at each node considered for integrating the weak form, it suffices to approximate the different components of the velocity field in each element by using standard shape functions, such as piecewise linear interpolants, and then to evaluate the integral on the boundary of the cell associated with each node. The cell being typically polyhedral (for example when considering the Voronoi cells), a numerical quadrature consisting of few integration points is used for evaluating the boundary integral on each face of the polyhedral cell.

It is important to note that it allows us to avoid the explicit calculation of the shape function derivatives.

## 3. Validation of the strategy

### 3.1. Revisiting PGD through a Poisson's problem

This first example analyzes the PGD solution of a Poisson's problem:

$$\begin{cases} \Delta u = f & \text{in} \quad \Omega = (0,2)\times(0,1) \\ u = 0 & \text{on} \quad x = 0 \\ u = 0 & \text{on} \quad y = 0 \\ u = -y(y-1) & \text{on} \quad x = 2 \\ \dfrac{\partial u}{\partial y} = g(x) & \text{on} \quad y = 1 \end{cases}$$

where the source term has been considered as

$$f(x,y) = -20\exp((1-x)^2/0.1)\exp((0.5-y)^2/0.1)$$

The function associated with natural boundary condition reads:

$$g(x) = \begin{cases} 0, \text{if } x \le 0.5 \\ 1, \text{if } x > 0.5 \end{cases}$$

The most typical structure of a PGD approximation to the problem is to look for a solution of the form:

$$u(x,y) \approx \sum_{i=1}^{N} F_i(x)\cdot G_i(y)$$

Here, a stopping criterion was set at $10^{-4}$ as tolerance for the residual. This leads around 40 PGD functional pairs or "modes", depending on the number of the 2D points considered. When new points are introduced, the solution becomes richer and more PGD modes are necessary to capture the finest solution features.

In Fig. 3, the absolute error (in infinity norm) of the PGD solution is presented. A 2D standard FEM solution in a fine-enough mesh was considered as a reference solution. Obviously, the more points are considered in the domain, the more information we get and the lesser error is obtained. This method is approximately of order one with respect to the number of points used.

The reference solution and the reconstructed PGD solution in the points of the 2D domain are presented in Fig. 4, where the reference solution is represented as a continuous surface and the PGD solution as spheres in the introduced points. The PGD solution is in very good agreement with the fully 2D solution, while it is computed only with the cost of a set of 1D problems.

### 3.2. Unsteady convection–diffusion equation

In this section the updated Lagrangian framework is considered and analyzed. For that purpose, the transient rotating pulse (advection–diffusion) example proposed in [2] is solved. The problem reads:

$$\begin{cases} u_t + \boldsymbol{a}\cdot\nabla u - \nabla\cdot(\nu\nabla u) = s & \text{in} \quad \Omega = (0,1)\times(0,1) \quad \text{(a)} \\ u = 0 & \text{on} \quad \partial\Omega \quad \text{(b)} \\ u = 0 & \text{at} \quad t = 0 \quad \text{(c)} \end{cases} \tag{8}$$

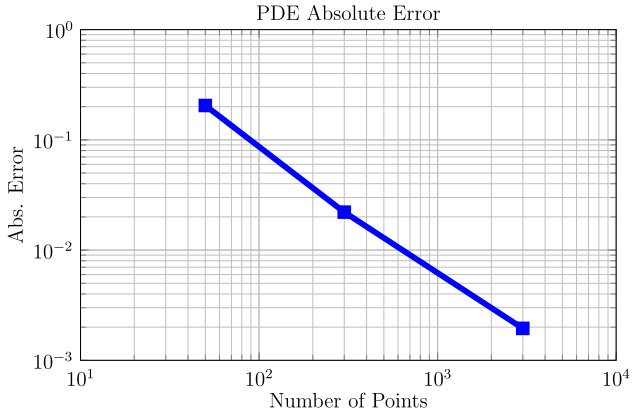


**Fig. 3.** PDE absolute error.

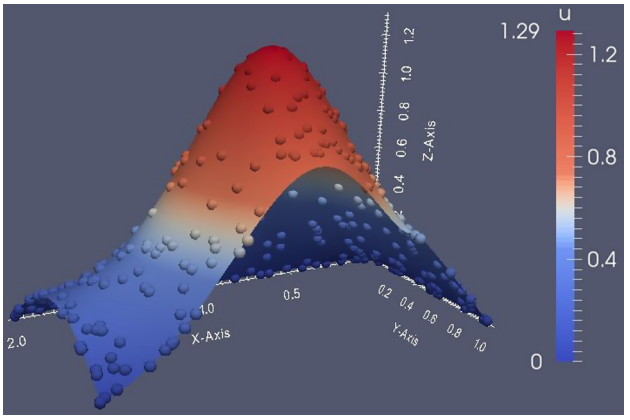


**Fig. 4.** Reference versus PGD solution.

with a small diffusion $\nu = 10^{-5}$, $\boldsymbol{a} = (-y + 0.5, x - 0.5)$ and

$$s = \begin{cases} \cos(\pi/2\sqrt{x_c^2 + y_c^2}), & \text{if } \sqrt{x_c^2 + y_c^2} \leq 1 \\ 0, & \text{otherwise} \end{cases}$$

with $(x_c, y_c) = (x - 0.2, y - 0.2)$.

It is well known that an Eulerian FEM solution requires stabilization regardless of the time integration scheme selected. Here we have used, as a reference solution, a streamline-upwind Petrov–Galerkin (SUPG) discretization in space and an implicit multistage Padé method $R_{2,2}$ as time integration scheme [2]. The stabilized weak form of the time discretized problem is given by

$$\left(w, \frac{\Delta \boldsymbol{u}}{\Delta t}\right) - (w, \boldsymbol{W}\, \Delta \boldsymbol{u}_t) + \sum_e (\boldsymbol{\tau}\mathcal{P}(w), \mathcal{R}(\Delta \boldsymbol{u}))_{\Omega^e} = \left(w, \boldsymbol{g} u_t^n\right)$$

where

$$\Delta \boldsymbol{u} = \begin{pmatrix} u^{n+\frac{1}{2}} - u^n \\ u^{n+1} - u^{n+\frac{1}{2}} \end{pmatrix} \qquad \Delta \boldsymbol{u}_t = \begin{pmatrix} u_t^{n+\frac{1}{2}} - u_t^n \\ u_t^{n+1} - u_t^{n+\frac{1}{2}} \end{pmatrix}$$

$\Delta \boldsymbol{u}$ is the primary variable, $w$ is the test function and $\Delta t$ the chosen time step. The partial time derivatives are obtained from the governing equation (8a),

$$u_t^n = s^n - \mathcal{L}(u^n)$$

where $\mathcal{L}$ is the associated linear differential operator.

The matrix $\boldsymbol{W}$ and the vector $\boldsymbol{g}$ are useful to express the Padé scheme in a compact form and read:

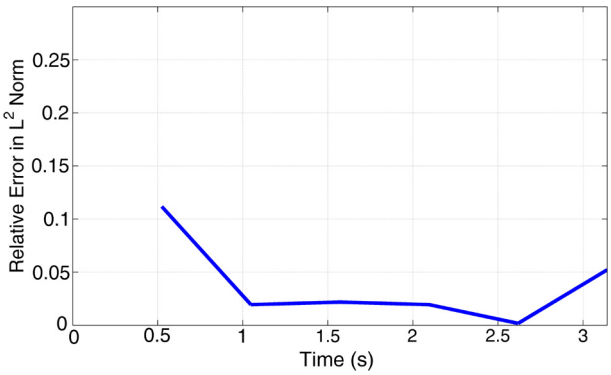


**Fig. 5.** Relative errors in $L^2$ norm.

$$\boldsymbol{W} = \frac{1}{24}\begin{pmatrix} 7 & -1 \\ 13 & 5 \end{pmatrix} \qquad \boldsymbol{g} = \frac{1}{2}\begin{pmatrix} 1 \\ 1 \end{pmatrix}$$

The operator $\mathcal{P}(w)$ characterizes the stabilization technique, in this case a SUPG,

$$\mathcal{P}(w) := \boldsymbol{W}(\boldsymbol{a}\cdot\nabla)w$$

The time-dependent residual $\mathcal{R}$ reads

$$\mathcal{R}(\Delta\boldsymbol{u}) = \frac{\Delta\boldsymbol{u}}{\Delta t} - \boldsymbol{W}\Delta\boldsymbol{u}_t - \boldsymbol{g}u_t^n$$

Finally, $\boldsymbol{\tau}$ is the intrinsic time scale matrix which in this example reads:

$$\boldsymbol{\tau} = \frac{h}{2a}\left[\coth(Pe) - \frac{1}{Pe}\right]\boldsymbol{W}^{-1}$$

where $h$ is the mesh size, $a$ is the convection magnitude and $Pe$ the Péclet number.

It is important to note that, even when using standard SUPG techniques, the solution exhibits oscillations near the boundary. In the updated Lagrangian approach, the convective term does not appear, and therefore stabilization is not necessary and oscillations naturally disappear. In an updated Lagrangian approach, the problem reads:

$$u_t - \nu\nabla^2 u = s$$

where $u_t$ represents the material derivative calculated along the flow streamlines related to the velocity field $\boldsymbol{a}$.

If an implicit temporal scheme is used, and the increment of $u$, $\Delta u = u^{n+1} - u^n$, is selected as primary variable, the semi-discretized equation to solve at each time step, reads:

$$\frac{\Delta u}{\Delta t} - \nu\nabla^2(\Delta u) = s^{n+1} + \nu\nabla^2 u^n$$

To solve this problem using the PGD, the trial and test functions are constructed as in the previous example, as

$$\Delta u(x,y) \approx \sum_{i=1}^{n-1} \Delta u_x^i(x)\cdot\Delta u_y^i(y) + R(x)\cdot S(y)$$

and

$$w = R^*(x)\cdot S(y) + R(x)\cdot S^*(y)$$

respectively. Moreover, in the time step $n+1$ the known fields $u^n$ and $s^{n+1}$ should be expressed in separated form by invoking a standard SVD.

This problem has been solved by the proposed strategy for different times in $[0,\pi]$ and compared with a reference FEM solution with no oscillations thanks to a higher diffusion coefficient. In Fig. 5, relative errors in $L^2$ norm for a value of the diffusion coefficient of $10^{-3}$ are presented. It can be seen that even with a number of points not too high (about 1000), the errors are small, between 2% and 10% throughout the complete simulation. These values are reasonable in an industrial context.

It is also remarkable that the method has a greater robustness in problems where convection is dominant. Indeed, if the diffusion coefficient is set to $10^{-5}$, the FEM solution presents oscillations near the boundary, regardless of the time integration scheme used [2]. However, it can be seen in Fig. 6 that the proposed strategy provides a solution that does not present these oscillations on the border. The SUPG solution is presented as a continuous surface while the PGD solution is presented with spheres at the material points positions. Moreover, thanks to the separation of variables, the problem solution exhibits roughly a 1D computational cost.

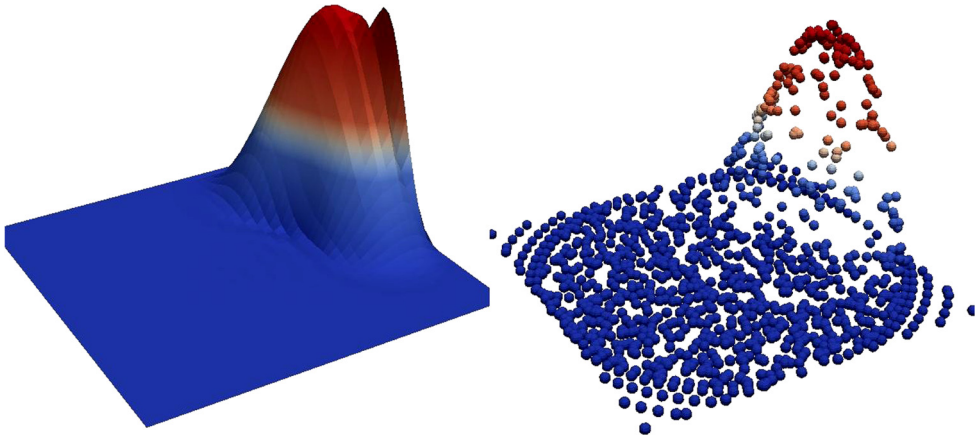

**Fig. 6.** FEM solution versus PGD solution in a convection-dominated problem.

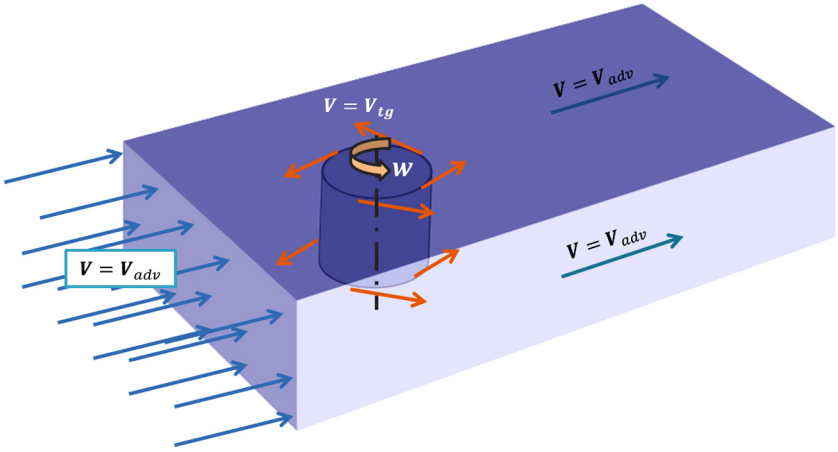


**Fig. 7.** FSW kinematics model.

## 4. FSW-like kinematics

FSW is a solid-state welding technique which, since its invention in 1991, is of great interest to the industry [23]. The FSW welding process is conceptually simple. A non-consumable rotating tool with a specially designed pin and shoulder is inserted into the abutting edges of sheets or plates to be joined and traversed along the line of joint. The tool heats the workpiece ant its stir movement produces the joint.

In this work, a simplified model of the kinematics of this process has been tested with the proposed strategy. The viscous flow expressed in Eq. (1) has been solved considering a non-linear behavior law (a power law, Eq. (4)). For the sake of simplicity and without loss of generality, the thermal problem has been omitted, considering an isothermal process without mechanical dissipation. The boundary conditions consists of an imposed velocity ($\boldsymbol{V}_{\text{adv}}$) far away from the tool ($\partial\Omega$) and of an imposed tangential velocity ($\boldsymbol{V}_{\text{tg}}$) at the tool surface ($\partial\Lambda$). In Fig. 7, a scheme of the problem is depicted. Thus, the problem reads,

$$\begin{cases} \nabla\cdot\boldsymbol{\sigma} = \boldsymbol{0} & \text{in} \quad \Omega \\ \nabla\cdot\boldsymbol{v} = 0 & \text{in} \quad \Omega \\ \boldsymbol{v} = \boldsymbol{V}_{\text{adv}} & \text{on} \quad \partial\Omega \\ \boldsymbol{v} = \boldsymbol{V}_{\text{tg}} & \text{on} \quad \partial\Lambda \end{cases}$$

Even when neither the real technological parameters (constitutive model, friction law, ...) nor the actual geometry of the tools are implemented, the feasibility of the numerical algorithm is proved: a 3D flow model can be solved in an updated Lagrangian framework with a computational cost characteristic of 2D simulations. Moreover, the thermomechanical history (mechanical history in this case) of the material particles is computed directly from the simulation. For instance, we can study the evolution of the viscosity of a material particle during the process. In Fig. 8, we can observe how the viscosity of the material particle decreases when it approaches the tool, where the strain rates are high due to the rotation of the pin.

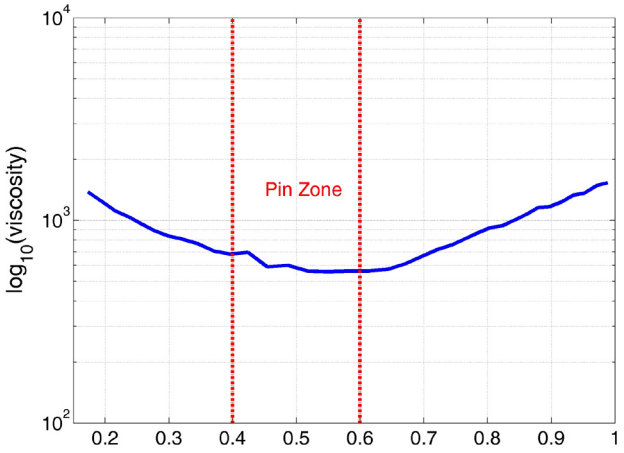


**Fig. 8.** Viscosity of a material particle with respect to the distance to the entrance.

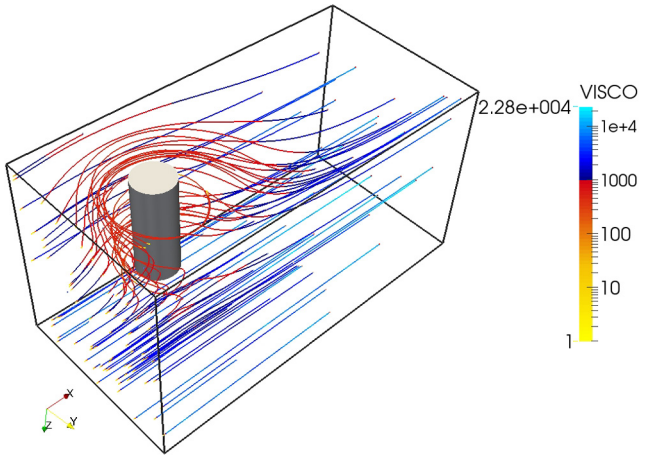


**Fig. 9.** Material viscosity along some material pathlines.

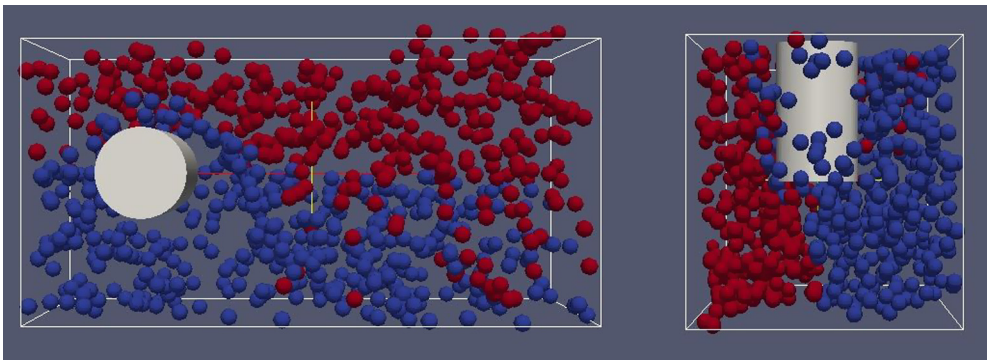

**Fig. 10.** Direct visualization of material mixing.

The streamlines are not computed *a posteriori*, they are simply the different positions of the material particles obtained during the simulation. In Fig. 9, the paths of some of these material points are shown. Moreover, it is well known from the literature [24] that the material flow play a fundamental role in the quality of the welding, and some typical defects such the tunnel effect can be predicted with its analysis. This method provides a direct way to perform this study; indeed the material particles of both welded plates are easily tracked just attaching an scalar value to them. In Fig. 10, this application is shown using two colors to represent the two different plates to joint. The relative position between the particles of the two plates behind the tool could indicate, using the appropriate techniques, the existence of defects.

## 5. Conclusions and perspectives

Simulation of material forming processes is one of these scenarios where traditional simulations encounter many difficulties. Recently, PGD appears as an appealing technique for reducing the computational complexity of models defined in 3D plate-like geometries. In this work, we proved that it is possible to combine the PGD with a robust integration method to create efficient updated Lagrangian simulations.

The examples presented prove the feasibility of the technique. The consideration of more realistic and complex processes with specific industrial application constitutes a work in progress.

## Acknowledgements

The authors wish to thank the ESI Group for its financial support through the *chaire industrielle* ESI Group–École centrale de Nantes. The work of Elías Cueto and Francisco Chinesta has been partially funded by the Spanish Ministry of Economy and Innovation through Grant number DPI2014-51844-C2-1-R. Francisco Chinesta also acknowledges the support of the Institut Universitaire de France.

## References

[1] President's Information Technology Advisory Committee, Computational science: ensuring America's competitiveness. Report to the President, June, 2005.
[2] Jean Donea, Antonio Huerta, Finite Element Methods for Flow Problems, John Wiley & Sons, 2003.
[3] Narges Dialami, Michele Chiumenti, Miguel Cervera, Carlos Agelet de Saracibar, An apropos kinematic framework for the numerical modeling of friction stir welding, Comput. Struct. 117 (0) (2013) 48–57.
[4] M.A. Martínez, E. Cueto, I. Alfaro, M. Doblaré, F. Chinesta, Updated Lagrangian free surface flow simulations with natural neighbour Galerkin methods, Int. J. Numer. Methods Biomed. Eng. 60 (13) (2004) 2105–2129.
[5] I. Alfaro, D. González, D. Bel, E. Cueto, M. Doblaré, F. Chinesta, Recent advances in the meshless simulation of aluminium extrusion and other related forming processes, Arch. Comput. Methods Eng. 13 (1) (2006) 3–44.
[6] I. Alfaro, J. Yvonnet, E. Cueto, F. Chinesta, M. Doblaré, Meshless methods with application to metal forming, Comput. Methods Appl. Mech. Eng. 195 (48–49) (2006) 6661–6675.
[7] I. Alfaro, D. Bel, E. Cueto, M. Doblaré, F. Chinesta, Three-dimensional simulation of aluminium extrusion by the alpha-shape based natural element method, Comput. Methods Appl. Mech. Eng. 195 (33–36) (2006) 4269–4286.
[8] A. Galavis, D. González, I. Alfaro, E. Cueto, Improved boundary tracking in meshless simulations of free-surface flows, Comput. Mech. (42) (2008) 467–479.
[9] E. Feulvarch, J.-C. Roux, J.-M. Bergheau, A simple and robust moving mesh technique for the finite element simulation of friction stir welding, J. Comput. Appl. Math. 246 (2013) (2013) 269–277.
[10] S. Guerdoux, L. Fourment, A 3D numerical simulation of different phases of friction stir welding, Model. Simul. Mater. Sci. Eng. 17 (7) (2009) 075001.
[11] J. Donea, A. Huerta, J. Ponthot, A. Rodriguez-Ferran, Arbitrary Lagrangian–Eulerian methods, in: E. Stein, R. de Borst, T.J.R. Hughes (Eds.), Encyclopedia of Computational Mechanics, Volume 1: Fundamentals, John Wiley & Sons, Ltd., 2004, pp. 1–38, Chap. 14.
[12] I. Alfaro, G. Racineux, A. Poitou, E. Cueto, F. Chinesta, Numerical simulation of friction stir welding by natural element methods, Int. J. Material Form. 2 (4) (2009) 225–234.
[13] Elias Cueto, Francisco Chinesta, Meshless methods for the simulation of material forming, Int. J. Material Form. (2013) 1–19.
[14] Francisco Chinesta, Roland Keunings, Adrien Leygue, The Proper Generalized Decomposition for Advanced Numerical Simulations: A Primer, in: Springer Publishing Company, Inc., 2013.
[15] Francisco Chinesta, Pierre Ladeveze, Elias Cueto, A short review on model order reduction based on proper generalized decomposition, Arch. Comput. Methods Eng. 18 (2011) 395–404.
[16] F. Chinesta, A. Ammar, E. Cueto, Recent advances in the use of the proper generalized decomposition for solving multidimensional models, Arch. Comput. Methods Eng. 17 (4) (2010) 327–350.
[17] Francisco Chinesta, Elias Cueto, PGD-Based Modeling of Materials, Structures and Processes, Springer International Publishing, Switzerland, 2014.
[18] Jiun-shyan Chen, Cheng-tang Wu, Sangpil Yoon, Yang You, A stabilized conforming nodal integration for Galerkin mesh-free methods, Int. J. Numer. Meth. Engng. 50 (2001) 435–466.
[19] W. Quak, A.H. Boogaard, D. González, E. Cueto, A comparative study on the performance of meshless approximations and their integration, Comput. Mech. 48 (2) (2011) 121–137.
[20] B. Bognet, F. Bordeu, F. Chinesta, A. Leygue, A. Poitou, Advanced simulation of models defined in plate geometries: 3D solutions with 2D computational complexity, Comput. Methods Appl. Mech. Eng. 201–204 (January 2012) 1–12.
[21] C. Ghnatios, F. Chinesta, C. Binetruy, 3D modeling of squeeze flows occurring in composite laminates, Int. J. Mater. Form. 8 (1) (2015) 73–83.
[22] Soo-Ik Oh, Taylan Altan, Metal Forming and the Finite-Element Method, Oxford University Press, 1989.
[23] R.S. Mishra, Z.Y. Ma, Friction stir welding and processing, Mater. Sci. Eng., R Rep. 50 (1–2) (2005) 1–78.
[24] J.A. Schneider, Temperature distribution and resulting metal flow, in: R. Mishra, R. Mahoney (Eds.), Friction Stir Welding and Processing, ASM International, 2007, Chapter 3.